Direct Quantification of Protein–Protein Interactions in Living Bacterial Cells

Soojung Yi, Eunji Kim, Sora Yang, Gyeongmin Kim, Da-Woon Bae, Se-Young Son, Bo-Gyeong Jeong, Jeong Seok Ji, Hyung Ho Lee, Ji-Sook Hahn, Sun-Shin Cha, Yeo Joon Yoon, and Nam Ki Lee**

Quantitative measurement of protein–protein interactions (PPIs) within living cells is vital for understanding their cellular functions at the molecular level and for applications in synthetic biology, protein engineering, and drug discovery. Although several techniques have been developed to measure PPI strength in vitro, direct measurement of PPI strength within living bacterial cells remains challenging. Here, a method for quantitatively measuring PPIs by determining the dissociation constant (K_d) in living *E. coli* using fluorescence resonance energy transfer (FRET), a technique termed KD-FRET, is reported. It is found that the direct excitation of the acceptor fluorophore among spectral crosstalks primarily results in non-interacting pairs exhibiting an apparent K_d, leading to false-positive signals. KD-FRET proves highly effective in quantifying various PPI K_d values, including both heterologous and homologous pairs. Moreover, KD-FRET enables the quantification of K_d for interaction pairs that are unmeasurable in vitro owing to their instability under standard buffer conditions. KD-FRET is successfully applied in the development of a novel synthetic biology tool to enhance naringenin production in *E. coli* and lycopene production in *S. cerevisiae* by precisely engineering metabolic pathway. These results demonstrate the potential of KD-FRET as a powerful tool for studying PPIs in their native cellular environments.

1. Introduction

The exploration of protein–protein interactions (PPIs) is a cornerstone of cellular biology, guiding essential processes that underpin various cellular functions.[1] Understanding the strength of binding interactions between proteins is crucial for elucidating cellular mechanisms, disease pathways, and developing therapeutic interventions targeting PPIs.[2,3] The dissociation constant (K_d) is a standard parameter that quantifies the binding affinity between interacting proteins. In vitro measurements of K_d under diluted conditions compared to the complex environment of living cells have been achieved using various techniques, such as surface plasmon resonance, fluorescence resonance energy transfer (FRET), and isothermal titration calorimetry (ITC).[4] However, the need to extend these investigations to living organisms is becoming apparent, as the intracellular environment differs significantly from in vitro conditions. Factors such as the highly crowded and heterogeneous nature of the cellular milieu, the presence of nonspecific weak interactions with other macromolecules, and dynamic cellular processes introduce challenges not encountered in vitro.[5,6] The potency of PPIs can vary significantly depending on the extent of crowding, even within in vitro environments, underscoring the importance of directly measuring these interactions within living cells.[7]

Several methods have been developed for observing PPIs in living cells. The yeast two-hybrid assay (Y2H) has been widely used for detecting PPIs because of its simplicity, although Y2H

S. Yi, S. Yang, J. S. Ji, H. H. Lee, N. K. Lee
Department of Chemistry
Seoul National University
1 Gwanak-ro, Gwanak-gu, Seoul 08826, Republic of Korea
E-mail: namkilee@snu.ac.kr

The ORCID identification number(s) for the author(s) of this article can be found under https://doi.org/10.1002/advs.202414777

DOI: 10.1002/advs.202414777

E. Kim, Y. J. Yoon
Natural Products Research Institute
College of Pharmacy
Seoul National University
1 Gwanak-ro, Gwanak-gu, Seoul 08826, Republic of Korea
E-mail: yeojoonyoon@snu.ac.kr

G. Kim, J.-S. Hahn
Department of Chemical and Biological Engineering
Institute of Chemical Processes
Seoul National University
1 Gwanak-ro, Gwanak-gu, Seoul 08826, Republic of Korea

D.-W. Bae, S.-Y. Son, B.-G. Jeong, S.-S. Cha
Department of Chemistry and Nanoscience
Ewha Womans University
52 Ewhayeodae-gil, Seodaemun-gu, Seoul 03760, Republic of Korea

often suffers from false-positive detection.[8] Fluorescence-based techniques, such as FRET, bioluminescence resonance energy transfer, and protein-fragment complementation assays, have also been widely applied for PPI detection in living cells.[9,10] Recently, in-cell NMR using isotope-labeled proteins has been developed for observing protein interactions.[5,11] Despite the growing importance of directly probing PPIs in living cells, the lack of suitable methods for assessing quantitative K_d values in live cells remains a significant barrier to progress in this field. Among the available techniques, FRET has been used as a promising tool for quantitatively measuring K_d in living cells, mostly in eukaryotic cells.[12] In addition to PPI measurements, quantitative FRET efficiency measurements, such as corrected FRET,[13] FRETN,[14] N_{FRET},[15] and QuanTI-FRET,[16] have been applied in eukaryotic cells.

However, FRET approaches for quantitative PPI measurements, as well as quantitative FRET efficiency measurements, in living bacterial cells are rare and less successful.[17] High autofluorescence backgrounds and more condensed conditions may be attributed to weak FRET signals in bacterial cells, resulting in a significant increase in false-positive interactions.[17] Previous studies assessed K_d within *E. coli* by measuring FRET signals collectively from heterogeneous cells, followed by disrupting cells using sonication and subsequent protein concentration measurement in vitro.[18] FRET efficiency has also been employed as an indicator of PPI.[19] However, FRET efficiency is dependent on the distance between two fluorescent proteins (FPs) and the concentrations of binder proteins, which limits its use as an indicator of binding affinity. As a result, it is highly demanding to develop a method for directly analyzing PPIs in living bacterial cells.

Here, we report a FRET-based method, termed KD-FRET, for quantitative PPI measurements in living *E. coli* cells, utilizing accurate FRET analysis. One fundamental limitation of using FRET for PPI measurements in bacterial cells is the weak FRET signals, which are often indistinguishable from background signals,[17] leading to false-positives. The strength of quantitative FRET measurements in in vitro single-molecule assays lies in their ability to distinguish weak FRET signals from background signals.[20,21] We adapted the in vitro single-molecule approach for use in live bacterial cells, enabling accurate correction of background noise and cross-talks between donor and acceptor fluorophores. This approach not only improved the reliability of FRET measurements in bacterial systems but also allowed for the quantification of K_d. We found that the direct excitation of the acceptor fluorophore is the major cause of false-positives in PPI measurements using FRET. Interestingly, the FRET efficiency of the standard sample was similar both in vitro and in living *E. coli* cells. Unlike previous approaches, KD-FRET allows the accurate determination of K_d values in living cells, including PPI pairs that are unstable or undetectable under standard in vitro conditions. Furthermore, we demonstrated the application of KD-FRET in synthetic biology by increasing naringenin production in *E. coli* and lycopene production in *S. cerevisiae* through the engineering of biosynthetic pathway using interaction protein pairs, as confirmed by our method. These findings underscore the potential of KD-FRET as a powerful tool for studying PPIs in their native cellular context and offering significant implications for both molecular biology and biotechnological applications.

2. Results and Discussion

2.1. Construction of Fluorescent Protein FRET Pairs for K_d Measurement

FP-fused PPI pair and their expression system are required to utilize FRET. The use of a single vector expressing the two fusion proteins for FRET-induced abnormal cellular growth. Thus, we chose two compatible vectors with different induction systems and antibiotic resistance genes.[22] In this study, pFF838, a chloramphenicol-resistant tetracycline-inducible vector, and pBBR6k, an ampicillin-resistant IPTG-inducible vector, were chosen as the donor and acceptor vectors, respectively (**Figure 1A**; Tables S1 and S2, Supporting Information). For FPs, a substantial overlap between the donor emission and acceptor excitation spectra increases the probability of energy transfer, thereby enhancing FRET efficiency (Figure 1B). However, this overlap also introduces spectral crosstalk, including leakage of donor emission into the acceptor detection channel and direct excitation of the acceptor by the donor excitation laser. These crosstalk effects can lead to false-positive FRET signals (Figure S1, Supporting Information). Therefore, the strength of crosstalk and bleed-through, maturation time, and FRET efficiency were considered (Figure 1B; Figures S1 and S2, Supporting Information). eGFP and mRFP were initially chosen as the FRET pair to minimize the crosstalk between FPs while maintaining considerable FRET efficiency. However, the eGFP-mRFP fused with a $(GGGS)_2$ linker yielded very low FRET efficiency. Thus, we used eGFPd, an eGFP C-terminal deletion mutant,[23] as the donor FP, which significantly increased FRET efficiency between eGFPd and mRFP (Figure S2C, Supporting Information). The excitation and emission maxima of eGFPd were at 486 and 512 nm, respectively, which were almost identical to those of eGFP (Figure S3, Supporting Information). eGFPd-$(GGGS)_2$-mRFP was used as a positive control for the high-FRET pair. Donor and acceptor expression vectors were transformed into *E. coli* BW25993 cells.

2.2. Quantification of the Intracellular Protein Concentration

Quantification of cellular protein concentrations is essential for measuring the K_d of PPIs. Traditionally, inferring the concentration of intracellular proteins has relied on the process of cell lysis.[5,18,24] However, we utilized the fusion of a protein of interest with a fluorescent reporter and leveraged imaging techniques to quantitatively determine both the number of proteins expressed and the volume of each cell (Figures S4 and S5, Supporting Information). We fused eGFPd or mRFP to the C-terminus of Tsr, a membrane protein transported to the inner membrane, and the fused gene was inserted in place of the native *lacZ* gene. After consecutive imaging, the fluorescent spots were photobleached sequentially. The intensities of single eGFPd and mRFP spots were obtained by subtracting the spot intensities before and after bleaching (Figure S4, Supporting Information).[25] The number of FPs in each cell was determined by dividing the total FP intensity by the intensity of a single FP. Then, the protein concentration of each cell was determined by the number of FP-fused protein divided by the cellular volume which was in turn calculated from the two-dimensional (2D) phase-contrast image of each cell.

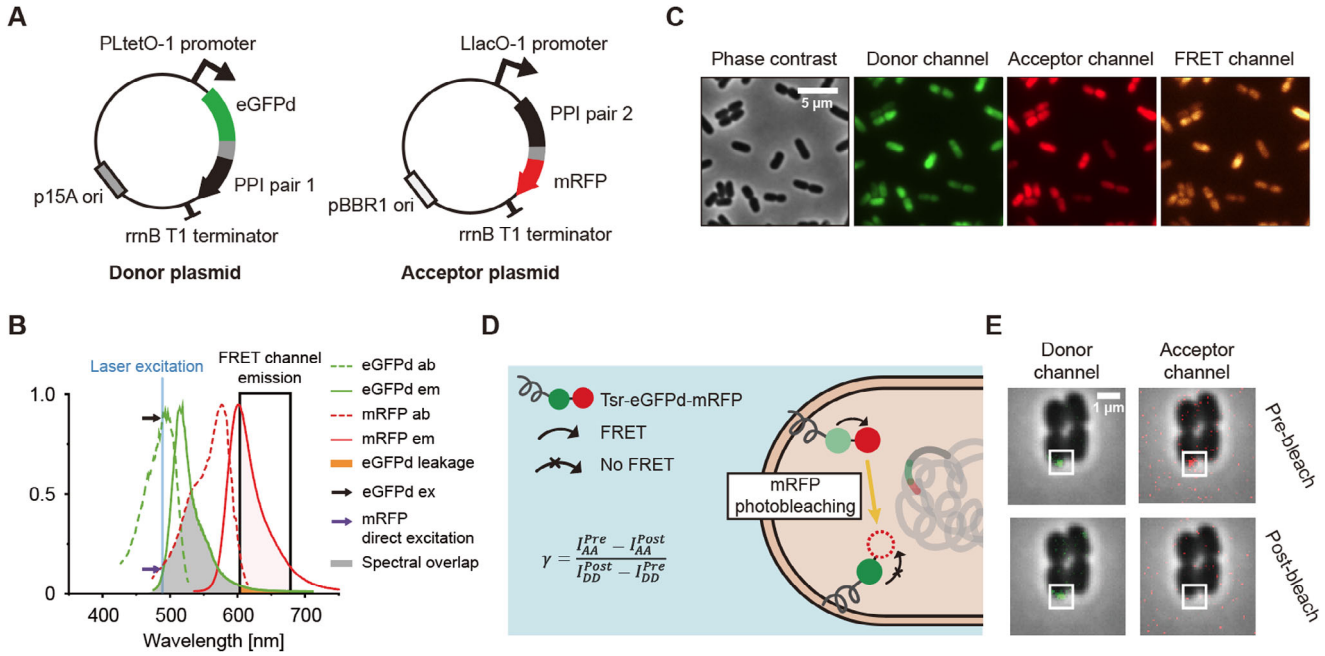

Figure 1. Schematic representation of the KD-FRET system in *E. coli*. A) Schematic of the two-vector system used for the concurrent expression of FRET donor and acceptor proteins. The donor plasmid expresses eGFPd fused to PPI pair 1, while the acceptor plasmid expresses mRFP fused to PPI pair 2. This system allows for independent and regulated expression of both fluorescent proteins in *E. coli* cells. B) Excitation and emission spectra of eGFPd and mRFP, the fluorescent proteins used in KD-FRET experiments. The green and red dashed lines represent the excitation spectra of eGFPd and mRFP, respectively, while the solid green and red lines represent their corresponding emission spectra. The blue line indicates the donor excitation wavelength (488 nm), and the black arrow represents the eGFPd excitation at this wavelength. The highlighted gray area indicates the spectral overlap between eGFPd emission and mRFP absorption, which facilitates energy transfer. The orange area represents the leakage of eGFPd emission into the FRET channel. The purple arrow indicates the direct excitation of mRFP by the 488 nm laser. C) Representative images from the three-channel FRET measurement system, showing *E. coli* cells imaged with phase contrast illumination, the donor channel (eGFPd), the acceptor channel (mRFP), and the FRET channel. Cells were imaged at 37 °C. The scale bar represents 5 µm. D) Schematic illustration of the Tsr-eGFPd-mRFP system used for calculating the γ factor. Prior to mRFP photobleaching, the eGFPd intensity is reduced due to FRET. After mRFP photobleaching, the eGFPd intensity increases as FRET is abolished. The γ factor is calculated by dividing the difference in acceptor intensity by the difference in donor intensity before and after mRFP photobleaching. E) Image of a fluorescent spot within a Tsr-eGFPd-mRFP expressing *E. coli* cell. The intensity of the fluorescent spot observed in the donor channel increases following mRFP photobleaching. The scale bar represents 1 µm.

2.3. Accurate FRET Analysis of KD-FRET for Living Bacterial Cells

The FRET efficiency can be measured using various techniques, such as sensitized emission, lifetime measurements, and acceptor photobleaching.[26] The accurate FRET measurement in single-molecule FRET has been developed based on sensitized emission FRET, the format of which is commonly available in most fluorescence microscopes equipped in cell biology laboratories.[27] Sensitized emission FRET measurements, also known as three-cube FRET or three-filter FRET,[28] consists of three detection channels: a donor channel (donor emission detection by donor excitation, I_{DD}), an acceptor channel (acceptor emission detection by acceptor emission, I_{AA}), and a FRET channel (acceptor emission detection upon donor excitation, I_{DA}) (Figure 1C). FRET efficiency (E) is calculated as follows:

$$E = \frac{I_{DA}}{I_{DA} + I_{DD}} \quad (1)$$

The backgrounds and noise signals must be properly corrected from I_{DD}, I_{AA}, and I_{DA} to obtain accurate FRET efficiency.

(Step 1) Subtraction of image background signals. Image background signals (hereafter "BG") should be removed. We measured the intensity of each image frame, i.e., I_{DD}^{BG}, I_{AA}^{BG}, and I_{DA}^{BG}.

(Step 2) Subtraction of cellular autofluorescence. Bacterial cells have autofluorescence. Wild-type BW25993 cells were used for autofluorescence correction of each channel.

(Step 3) Leakage correction. The use of two different FPs for FRET measurements inevitably resulted in spectral crosstalk. Specifically, leakage (Lk) refers to the unintended detection of donor fluorescence by the acceptor channel, while direct excitation refers to the excitation of the acceptor fluorophore directly by donor excitation. Leakage or direct excitation can generate false FRET signals. Therefore, correction of these two factors is important for obtaining appropriate FRET signals. The contribution of Lk can be determined using *E. coli* cells transformed with plasmids expressing donor proteins (hereafter "Donly") by dividing the FRET channel intensity (I_{DA}^{Donly}) by the donor channel intensity (I_{DD}^{Donly}).

(Step 4) Direct excitation correction. The direct excitation (Dir) can be corrected by using *E. coli* cells expressing acceptor proteins (hereafter "Aonly"): the FRET channel intensity (I_{DA}^{Aonly}) was divided by the acceptor channel intensity (I_{AA}^{Aonly}).

The FRET intensity of the FRET sample (I_{DA}^{FRET}) was then corrected by eliminating leakage and direct excitation using the following equation:

$$Corrected\ FRET,\ F^{FRET} = I_{DA}^{FRET} - \left(Lk{*}I_{DD}^{FRET}\right) - \left(Dir{*}I_{AA}^{FRET}\right) \quad (2)$$

(Step 5) Gamma (γ) factor correction. The γ factor, also known as the detection efficiency correction factor, accounts for the difference in detection efficiency between the donor and acceptor channels. The γ factor can be obtained by measuring the intensity changes of the immobilized single donor–acceptor fusion protein before and after acceptor photobleaching, $\gamma = \frac{\Delta I_{AA}}{\Delta I_{DD}}$ (Figure 1D).[29] To obtain γ factor using the microscope, the membrane protein Tsr-fused eGFPd-mRFP tandem protein was expressed from chromosomally integrated *tsr-eGFPd-mRFP* gene (SY004 strain). The change in the intensity of a membrane-localized eGFPd-mRFP spot upon mRFP photobleaching was measured in both donor and acceptor channels. The spot intensity of the donor channel increased after mRFP was photobleached, owing to the destruction of the FRET acceptor (Figure 1D,E). The distribution of γ factor was obtained from the intensities of the eGFPd-mRFP spot before (*pre*) and after (*post*) mRFP photobleaching (Figure 1D). The γ factor was measured to be 0.45 ($n = 31$) by fitting the distribution to a Gaussian function.

Finally, FRET efficiency (E) was calculated using the following equation:

$$E = \frac{F^{FRET}}{F^{FRET} + \gamma{*}I_{DD}^{FRET}} \quad (3)$$

(Step 6) Outlier removal. The emergence of outliers with either negative or extremely large FRET efficiency values is inevitable due to a series of noise correction procedures.[30] Therefore, it is often required to establish a threshold for outlier removal. Given that outliers are frequently associated with low intracellular donor concentrations (weak donor signals), we used a threshold based on the mean donor channel intensity subtracted by its standard deviation.[31] Cells exhibiting donor channel intensities below this threshold were considered outliers and excluded from the analysis.

(Step 7) Dissociation constants. After applying all the correction procedures, individual cells were binned according to their intracellular acceptor concentrations. The donor concentration and FRET efficiency in each bin were averaged and plotted. Consequently, the data were fitted using a quadratic binding equation to determine the K_d values (Figure S6, Supporting Information).[32] The plots fitted using the quadratic binding equation are shown as 2D plots instead of 3D plots for simplicity. The overall workflow is summarized in Figure S7 (Supporting Information).

2.4. Validation of KD-FRET Using the Positive and Negative Controls in Living Bacterial Cells

Each correction step was then applied to the positive and negative controls of the FRET pairs to determine K_d. As a negative control, we expressed both eGFPd and mRFP using two different vectors, respectively. The negative control should result in a FRET efficiency value close to zero after full correction, and its K_d should not be measured because there is no interaction between the FPs. The directly fused eGFPd and mRFP (eGFPd-$(GGGS)_2$-mRFP) was used as a positive control, with its FRET efficiency expected to be independent of eGFPd-mRFP concentration. K_d cannot be determined for eGFPd-mRFP, as it represents a case of an infinite association constant.

Figure 2A shows the FRET efficiency and K_d measurements at each correction step for negative controls. Notably, after step 1 correction, false interactions were observed with $K_d = 2.82 \pm 0.62 \times 10^{-6}$ M. The FRET efficiency, indicating the interaction between eGFPd and mRFP, initially increased as the concentration of the acceptor protein (mRFP) increased within the cell, yielding a positive E value and pseudo-K_d (Figure 2B,C). Until step 3 of the leakage correction, the false-positive K_d was measured to be $2.26 \pm 0.42 \times 10^{-6}$ M. Interestingly, however, after step 4 direct excitation correction, a false-positive K_d was not detected. The FRET efficiency was also close to zero after step 4 correction. These results indicate that the false-positive result for protein interaction using FRET pairs in living bacterial cells mostly comes from the crosstalk of direct excitation. To evaluate the effect of direction excitation correction, we applied it in step 3, followed by leakage correction in step 4 (Figure S8, Supporting Information). Again, the direct excitation correction removed the false-positive K_d value. These results clearly demonstrate that the false-positive K_d measurement occurs in living bacterial cells due to the spectral crosstalk. It is essential to perform direction excitation correction, even for fast qualitative screening for PPI pairs in living *E. coli* using FRET, to remove the false-positive results. We further validated the importance of direct excitation correction using another non-interacting pair (eGFPd and $^{N}DD_{MlnC}$-mRFP), which similarly showed elimination of false-positive signals after proper correction (Figure S9, Supporting Information). Meanwhile, γ factor correction and outlier removal are not essential for K_d measurement using FRET.

The results of the positive FRET control are presented in Figure 2B,C. As predicted, the FRET efficiency was independent of the FP concentration and K_d was not determined. After full correction to step 6, the FRET efficiency was measured to be 0.16 ± 0.02 for eGFP-mRFP in living *E. coli*. The results of the positive control also support the robustness of our correction processes.

2.5. Comparison of the FRET Efficiencies Measured In Vitro and in Living Cells

It has been an interesting question whether the FRET efficiencies measured in vitro matches those measured in living cells.[33] Therefore, we compared the FRET efficiency of the positive control measured in living cells to that measured in vitro. To determine the FRET efficiency in vitro, we used the sensitized-emission FRET measurement with correction of all crosstalks.[20,34] We determined the extinction coefficients of the purified free eGFPd and free mRFP at the identical wavelength to KD-FRET measurement (488 nm for eGFPd excitation, 580 nm for mRFP excitation), which were 58 705.8 M^{-1} cm^{-1} ($\varepsilon_{488\ nm}^{eGFPd}$) and 53 000 M^{-1} cm^{-1} ($\varepsilon_{580\ nm}^{mRFP}$), respectively. As a result, the in vitro FRET efficiency of the positive control was measured to be 0.20 ± 0.03 by using a fluorometer, which is in a similar range as the

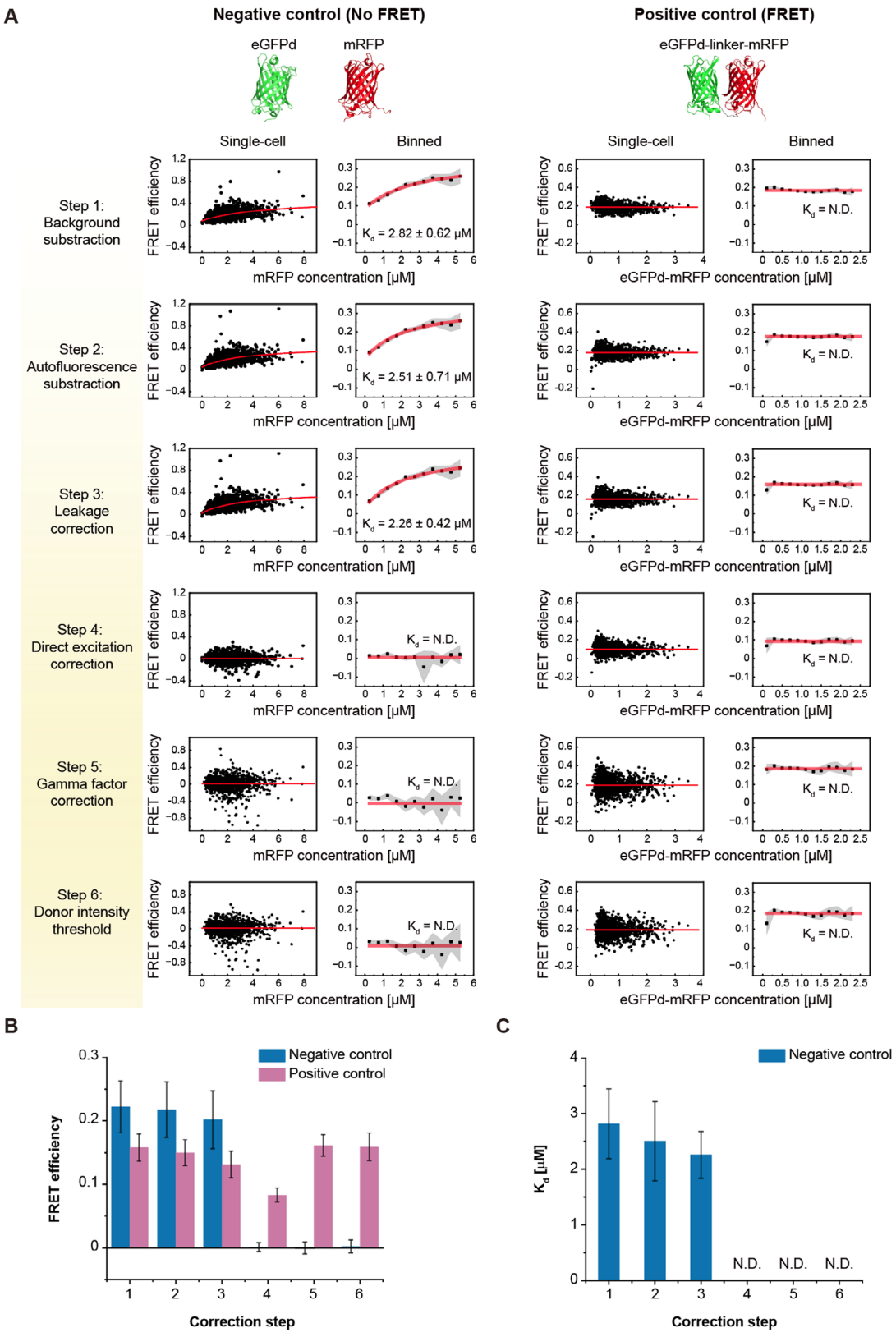

Figure 2. Stepwise correction of FRET efficiency and its impact on K_d measurements in *E. coli* cells. A) Data analysis processes and corresponding single-cell and binned scatter plots for negative (left) and positive (right) controls. The plots depict the step-by-step correction of FRET efficiency, including background subtraction, autofluorescence subtraction, leakage correction, direct excitation correction, γ factor correction, and donor intensity

FRET efficiency of living cells (0.16 ± 0.02). These results indicate that FRET efficiency quantitatively measured in vitro closely mirrors that observed in living *E. coli* cells. This comparative result further supports the robustness of our analytical approach for determining intracellular FRET efficiency.

2.6. Dissociation Constant Measurements of Known Interaction Pairs by KD-FRET

Then, to confirm the robustness of KD-FRET, we employed a well-characterized PPI system consisting of docking domains (DDs) from polyketide synthases (PKS). DDs of PKSs are positioned at the C- and N-termini of PKSs, interacting exclusively with their designated pairs and ensuring the organization of the multienzyme complex.[21,22] We chose the C-terminal DD ($^{C}DD_{MlnB}$) and N-terminal DD ($^{N}DD_{MlnC}$) derived from macrolactin *trans*-AT PKS, MlnB/MlnC and MlnD/MlnE, whose interaction is characterized by the formation of a four-helix bundle, with complementary branched-chain amino acids at the core interface mediating specific recognition and stabilizing the complex assembly (**Figure 3A**).[35] The K_d values, reported as 2.9 ± 1.1 × 10^{-6} and 4.8 ± 2.3 × 10^{-6} M, were measured in vitro using FRET without applying crosstalk corrections.[36]

We directly measured the K_d values of $^{C}DD_{MlnB}$/$^{N}DD_{MlnC}$ and $^{C}DD_{MlnD}$/$^{N}DD_{MlnE}$ pairs within the cellular context by utilizing our FRET measurement system (Figure 3B). $^{C}DD_{MlnB}$ and $^{C}DD_{MlnD}$ were labeled with eGFPd, whereas $^{N}DD_{MlnC}$ and $^{N}DD_{MlnE}$ were labeled with mRFP. The FP-labeled $^{C}DD_{MlnB}$/$^{N}DD_{MlnC}$ and $^{C}DD_{MlnD}$/$^{N}DD_{MlnE}$ pairs were expressed using two vector systems (Figure 1A). We applied the correction until step 6 for K_d determination. The K_d values for $^{C}DD_{MlnB}$/$^{N}DD_{MlnC}$ and $^{C}DD_{MlnD}$/$^{N}DD_{MlnE}$ pairs in living *E. coli* were measured to be 2.29 ± 1.28 × 10^{-6} and 0.25 ± 0.08 × 10^{-6} M, respectively (Figure 3B). To confirm whether the measured K_d values were reasonable, we purified the identical fusion proteins and measured their K_d values using FRET in vitro. The K_d values for $^{C}DD_{MlnB}$/$^{N}DD_{MlnC}$ and $^{C}DD_{MlnD}$/$^{N}DD_{MlnE}$ pairs were 5.66 ± 1.52 × 10^{-6} and 1.50 ± 0.46 × 10^{-6} M, respectively (Figure 3C). Furthermore, we measured the K_d value of $^{C}DD_{MlnB}$/$^{N}DD_{MlnC}$ pair using ITC, which yielded a value of 6.85 ± 0.41 × 10^{-6} M (Figure S10, Supporting Information). The in-cell K_d values obtained through KD-FRET measurements closely matched those obtained through in vitro measurements, providing additional support for the reliability of our methodology. The difference in K_d values between in vitro and in-cell assays may be due to the complex nature of the intracellular environment. Factors such as macromolecular crowding, increased viscosity, nonspecific interactions with other macromolecules, and enhanced protein stability in the cellular milieu may collectively contribute to the observed differences, resulting in lower K_d values in cells.[5,37,38]

2.7. K_d of UvrA/UvrB Interacting Pair in living *E. Coli* Cells

To broaden the spectrum of protein–protein interaction pairs amenable to K_d measurements using our approach, we measured the in-cell K_d of the UvrA/UvrB protein-protein interaction pair, a relatively large protein complex related to nucleotide excision repair within *E. coli*. UvrA and UvrB proteins interact with each other in a 1:1 ratio to form the $UvrA_2B_2$ complex having in vitro $K_d \approx 0.8 \times 10^{-6}$ M determined by isothermal titration calorimetry (**Figure 4A**).[39] The expression of UvrA/UvrB pair was prepared using the two-vector system (Figure 1A), and the vectors were transformed into the UvrA/UvrB knockout BW25993 cells. We also performed the correction until step 6 to determine K_d. As a result, in cell K_d of UvrA/UvrB pair was measured as 0.17 ± 0.13 × 10^{-6} M (Figure 4B,C). These data show that our method can be applied not only to small heterologous protein pairs, but also to large PPI pairs in *E. coli*.

2.8. Measurement of K_d Values of PPI Pairs That are Unmeasurable In Vitro

Given that PPIs are highly influenced by their surrounding environment, the affinity of these interactions may vary depending on the type of reaction buffer used or may not be measurable consistently in vitro.[3,40] For example, several studies have shown that ion concentration and the type of buffer used alter PPIs, even at physiological pH.[41] In our study, the DD pairs of TarE/TarF and ElaJ/ElaK, known to interact,[42] exhibited either unstable interactions or undetectable K_d values in vitro (Figure S11, Supporting Information). However, our approach directly measured the K_d values within living *E. coli* cells, i.e., 1.49 ± 0.79 × 10^{-6} and 1.18 ± 0.79 × 10^{-6} M for $^{C}DD_{TarE}$–$^{N}DD_{TarF}$, $^{C}DD_{ElaJ}$–$^{N}DD_{ElaK}$ pairs, respectively (**Figures 5A** and S12, Supporting Information). KD-FRET appears to provide a reliable assessment of binding affinities, free from potential artifacts due to the quality of the purified proteins and different buffer conditions, although further investigation is still required. This result further highlights the value of quantifying protein interaction strength within a cellular context.

2.9. Application of the PKS Interaction Pairs Analyzed in Living Cells for Synthetic Biology

A metabolon refers to a dynamic and intricately organized protein complex comprising enzymes involved in specific metabolic pathways.[43] This molecular assembly enhances the efficiency of biochemical reactions within a given metabolic pathway. It facilitates the sequential conversion of metabolites by channeling intermediates from one enzyme to the next. Metabolic engineering, aimed at enhancing the efficient production of desired substances, could potentially benefit from emulating the concept of

thresholding. In the negative control, incomplete corrections resulted in scatter plots displaying a binding curve shape, leading to false-positive K_d values. In the positive control, the absence of γ factor correction led to an underestimation of FRET efficiency compared to in vitro FRET measurements of the purified positive control. K_d values are reported as mean ± standard deviation (SD) of triplicates. The gray-shaded regions represent the 95% confidence intervals for the binned mean FRET efficiency. B) Analysis of FRET efficiency values and C) K_d for the negative (blue) and positive (red) controls across the correction steps. The data highlight how each correction step affects the accuracy of the K_d and FRET efficiency measurements, emphasizing the importance of correction processes for reliable in-cell FRET analysis. Error bars were obtained from the SDs of three independent measurements. N.D.: Not determined.

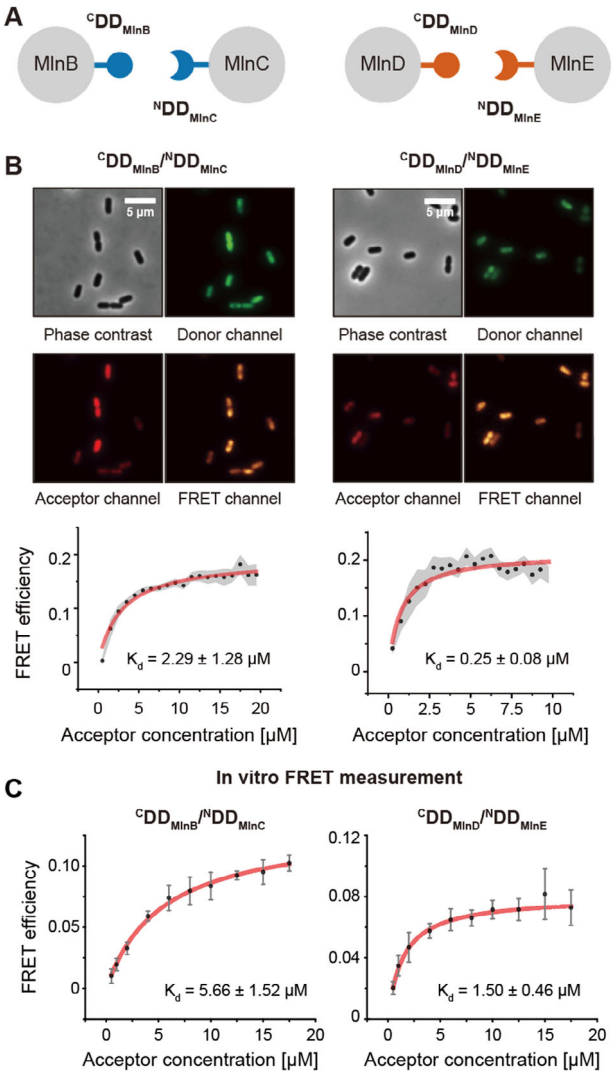

Figure 3. K_d determinations in living cells and in vitro using accurate FRET measurements. A) Schematic representation of the interactions between docking domains (DDs) from the macrolactin trans-AT polyketide synthases (PKSs) MlnB/MlnC and MlnD/MlnE. The C-terminal DDs (^{C}DD) and N-terminal DDs (^{N}DD) from MlnB–MlnC and MlnD–MlnE specifically interact with their corresponding partners, forming well-defined protein–protein interaction (PPI) pairs. B) Representative in-cell K_d measurements of $^{C}DD_{MlnB}/^{N}DD_{MlnC}$ (left) and $^{C}DD_{MlnD}/^{N}DD_{MlnE}$ (right) in living *E. coli* cells using KD-FRET. Fluorescence microscopy images show cells in phase contrast, donor channel (eGFPd), acceptor channel (mRFP), and FRET channel. The corresponding FRET efficiency versus acceptor concentration plots are presented below, with K_d values determined to be 2.29 ± 1.28 × 10^{-6} M for $^{C}DD_{MlnB}/^{N}DD_{MlnC}$ and 0.25 ± 0.08 × 10^{-6} M for $^{C}DD_{MlnD}/^{N}DD_{MlnE}$ (mean ± SD). Measurements were performed in triplicate at 37 °C. The gray-shaded regions represent the 95% confidence intervals for the binned mean FRET efficiency. The scale bar represents 5 μm. C) Representative in vitro K_d measurements of the same PPI pairs, $^{C}DD_{MlnB}/^{N}DD_{MlnC}$ (left) and $^{C}DD_{MlnD}/^{N}DD_{MlnE}$ (right), conducted with purified proteins in PBS buffer using a plate reader. The in vitro K_d values were measured to be 5.66 ± 1.52 × 10^{-6} M for $^{C}DD_{MlnB}/^{N}DD_{MlnC}$ and 1.50 ± 0.46 × 10^{-6} M for $^{C}DD_{MlnD}/^{N}DD_{MlnE}$ (mean ± SD). Measurements were performed in triplicate at 37 °C.

a metabolon. It may be possible to further increase the production yields by bringing enzymes into a closer proximity, similar to a metabolon.[44]

The biosynthesis of (2RS)-naringenin, a predominant member and fundamental building block of diverse flavonoids, involves the enzymatic conversion of *p*-coumaric acid to 4-coumaroyl-CoA by 4-coumaroyl-CoA ligase (4CL), followed by the formation of naringenin chalcone from 4-coumaroyl-CoA catalyzed by chalcone synthase (CHS). Naringenin chalcone undergoes a spontaneous conversion to (2RS)-naringenin (Figure 5B).[45] In the cellular context, these enzymes are independently expressed, existing without specific organization within the cell, and solely depending on diffusion for interaction. We used the $^{C}DD_{MlnB}/^{N}DD_{MlnC}$ or $^{C}DD_{MlnD}/^{N}DD_{MlnE}$, whose K_d values have been determined in living *E. coli* by our KD-FRET method, to co-localize the 4CL and CHS enzymes and improve biocatalytic efficiency of flavonoid production in *E. coli*. The ^{C}DDs were tagged to the C terminus of 4CL, while the ^{N}DDs were attached to the N terminus of CHS (Figure 5B), facilitating enzyme assembly via selective interactions between the cognate DD pairs. To evaluate the influence of 4CL and CHS on enzymatic activity and expression levels within cells when fused to DD pairs, control strains containing only a single DD tag were also constructed (Table S3, Supporting Information). The strain NAR_{MlnB} (harboring 4CL-$^{C}DD_{MlnB}$) produced less naringenin than the strain NAR_{Free}, which possesses untagged 4CL and CHS. In contrast, the strains NAR_{MlnC}, NAR_{MlnD}, and NAR_{MlnE} (containing $^{N}DD_{MlnC}$-CHS, 4CL-$^{C}DD_{MlnD}$, and $^{N}DD_{MlnE}$-CHS, respectively) exhibited a modest enhancement in naringenin production relative to the strain NAR_{Free}. In our previous study, we observed that DD tagging did not influence enzymatic activity of the 4CL or CHS.[35] Therefore, the differences in production among the control strains are presumed to result from differences in the expression levels of the fusion proteins. As a result, the assembly strains ($NAR_{MlnB\text{-}C}$ and $NAR_{MlnD\text{-}E}$) produced higher amount of naringenin than the control strains, likely attributable to the influence of DD-based substrate channeling. Interestingly, the assembly strain utilizing $^{C}DD_{MlnB}/^{N}DD_{MlnC}$, exhibiting a K_d value of 2.29 ± 1.28 × 10^{-6} M, showed a 4.1-fold increase in naringenin production (Figure 5C). Furthermore, another assembly strain utilizing $^{C}DD_{MlnD}/^{N}DD_{MlnE}$, exhibiting a stronger interaction with a K_d of 0.25 ± 0.08 × 10^{-6} M, showed a remarkable 25.5-fold increase in naringenin production compared to NAR_{Free} strain (Figure 5C). These results indicate that the biocatalytic efficiency of the artificial metabolon is enhanced when using PPI domain pairs with lower K_d values.

However, this approach may not be universally applicable across all metabolic pathways. To explore whether the PPI domain interactions observed in *E. coli* could be transferred to other host organisms, we applied the $^{C}DD_{MlnB}/^{N}DD_{MlnC}$ pair within the lycopene biosynthetic pathway in genetically engineered *Saccharomyces cerevisiae*. The pathway was constructed by integrating the *tHMG1* and *crtI* genes (encoding hydroxymethylglutaryl-CoA reductase and phytoene desaturase, respectively) onto the *S. cerevisiae* chromosome. In addition, the *erg20* gene (encoding farnesyl pyrophosphate synthase) and *crtE* gene (encoding geranylgeranyl pyrophosphate synthase) were co-expressed along with the *crtB* gene (encoding phytoene synthase) on a replicative plasmid, resulting in the strain LYC_{Free} (Figure 5D and Table S3, Support-

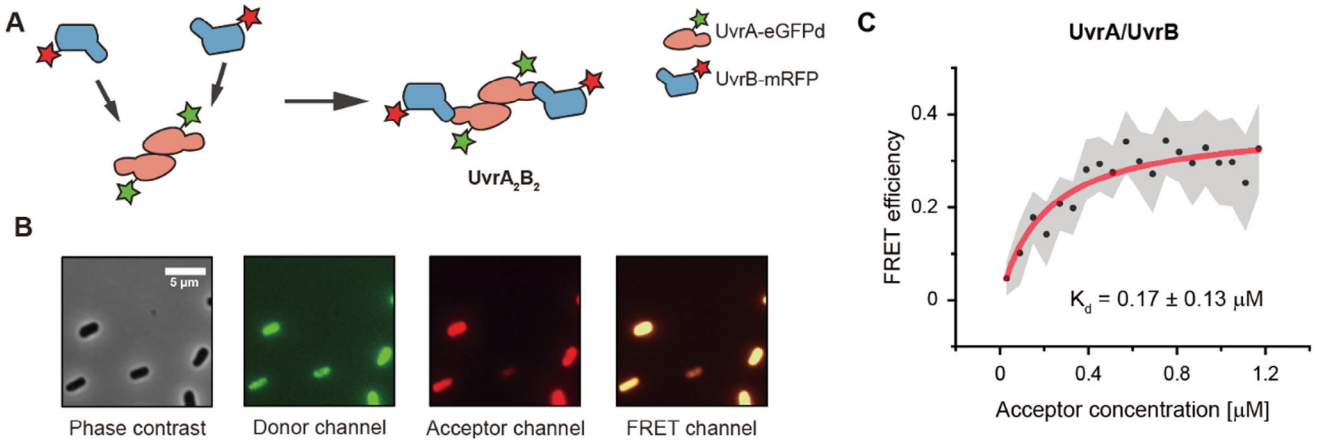

Figure 4. In-cell K_d determination of the UvrA/UvrB interaction using KD-FRET in living *E. coli*. A) Schematic representation of the UvrA/UvrB protein–protein interaction. UvrA is labeled with eGFPd, and UvrB is labeled with mRFP. These proteins interact in a 1:1 stoichiometry to form the $UvrA_2B_2$ complex. B) Fluorescence microscopy images showing the expression of UvrA-eGFPd and UvrB-mRFP in the *E. coli* BW25993 strain, which has a double deletion of the uvrA and uvrB genes. The scale bar represents 5 µm. C) Representative in-cell K_d measurement for the UvrA/UvrB interaction performed at 37 °C. The FRET efficiency is plotted against acceptor concentration, and the K_d value was determined to be $0.17 \pm 0.13 \times 10^{-6}$ M from three independent measurements (mean ± SD). The gray-shaded regions represent the 95% confidence intervals for the binned mean FRET efficiency.

ing Information). We selected ERG20 and CrtE as target enzymes to be assembled in a lycopene-producing yeast host, anticipating that efficient substrate channeling among C5, C10, and C15 intermediates would be facilitated, leading to enhanced lycopene production. The $^{C}DD_{MlnB}$ and $^{N}DD_{MlnC}$ were fused to the N termini of CrtE and ERG20, respectively, resulting in strain $LYC_{MlnB\text{-}C}$, which comprises $^{C}DD_{MlnB}$-CrtE and $^{N}DD_{MlnC}$-ERG20. Control strains containing one of the tags with no assembly functionality were also constructed (Table S3, Supporting Information). Lycopene production in the assembly strain was 3.4-fold higher than in the untagged control strain (Figure 5E). The DD-tagging of either CrtE or ERG20 alone in the control strains did not significantly affect lycopene production. These results showed that the efficacy of the artificial metabolon was preserved when the identical PPI domain pair was utilized in metabolic pathways in different host organisms.

Our results demonstrate that utilizing KD-FRET enables the screening of interactions in living cells more efficiently, providing a more streamlined approach for constructing artificial metabolons.

3. Discussion

Despite the importance of PPIs, direct methods to measure their strength in living *E. coli* cells have been lacking, largely due to high autofluorescence and the complexity of the cellular environment. Furthermore, it is known that intracellular FRET and NMR signals used to observe PPIs in *E. coli* typically exhibit broader distributions and lower signal-to-noise ratios compared to those in other organisms.[17,46] The dense intracellular environment of *E. coli* may contribute to the reduced diffusivity of proteins and variations in FRET efficiency, complicating quantitative K_d measurements.[47] Although in vitro studies provide valuable insights, they often fail to replicate the intracellular milieu, highlighting the need for in-cell approaches. Our work presents a FRET-based method for quantitatively measuring K_d values of PPIs directly within living *E. coli* cells. This method overcomes previous challenges by eliminating the need for protein purification and allowing measurements in a natural cellular context. The use of correction factors in KD-FRET significantly reduced false-positives, enhancing the reliability of FRET efficiency measurements. This technique can address the instability of PPIs in in vitro conditions by measuring them directly within the cellular environment.

Compared to other methods for measuring PPIs in bacterial cells, KD-FRET offers distinct advantages. The bacterial two-hybrid (B2H) system detects PPIs qualitatively rather than quantitatively and often requires genetic modifications that may alter the native interaction environment.[10,48] In-cell NMR provides atomic-level resolution but has limited applicability due to complex sample preparation steps, such as isotope labeling and reintroducing labeled proteins into cells via electroporation, as well as the need for specialized NMR equipment.[11,46,49] In contrast, KD-FRET is more accessible, requiring only a conventional fluorescence microscope and routine cloning for sample preparation. Traditional FRET-based approaches can detect PPIs but suffer from reduced sensitivity in bacterial cells due to background autofluorescence and broad/low FRET signals.[17] KD-FRET overcomes these limitations, enabling quantitative K_d measurements.

Minimizing autofluorescence inherent to growth media is crucial for detecting weak FRET signals. Rich media, such as Luria-Bertani broth, produce a high autofluorescence background. Therefore, KD-FRET experiments were conducted in minimal M9 media to reduce autofluorescence. In addition, a two-vector system was employed to independently regulate donor and acceptor protein expression levels by varying inducer concentrations. These strategies allowed control of protein expression levels within the expected K_d range, facilitating quantitative FRET efficiency measurements from the weak FRET signal of *E. coli* cells. As described before, autofluorescence, leakage, direct excitation, and γ-factor corrections were applied during every imag-

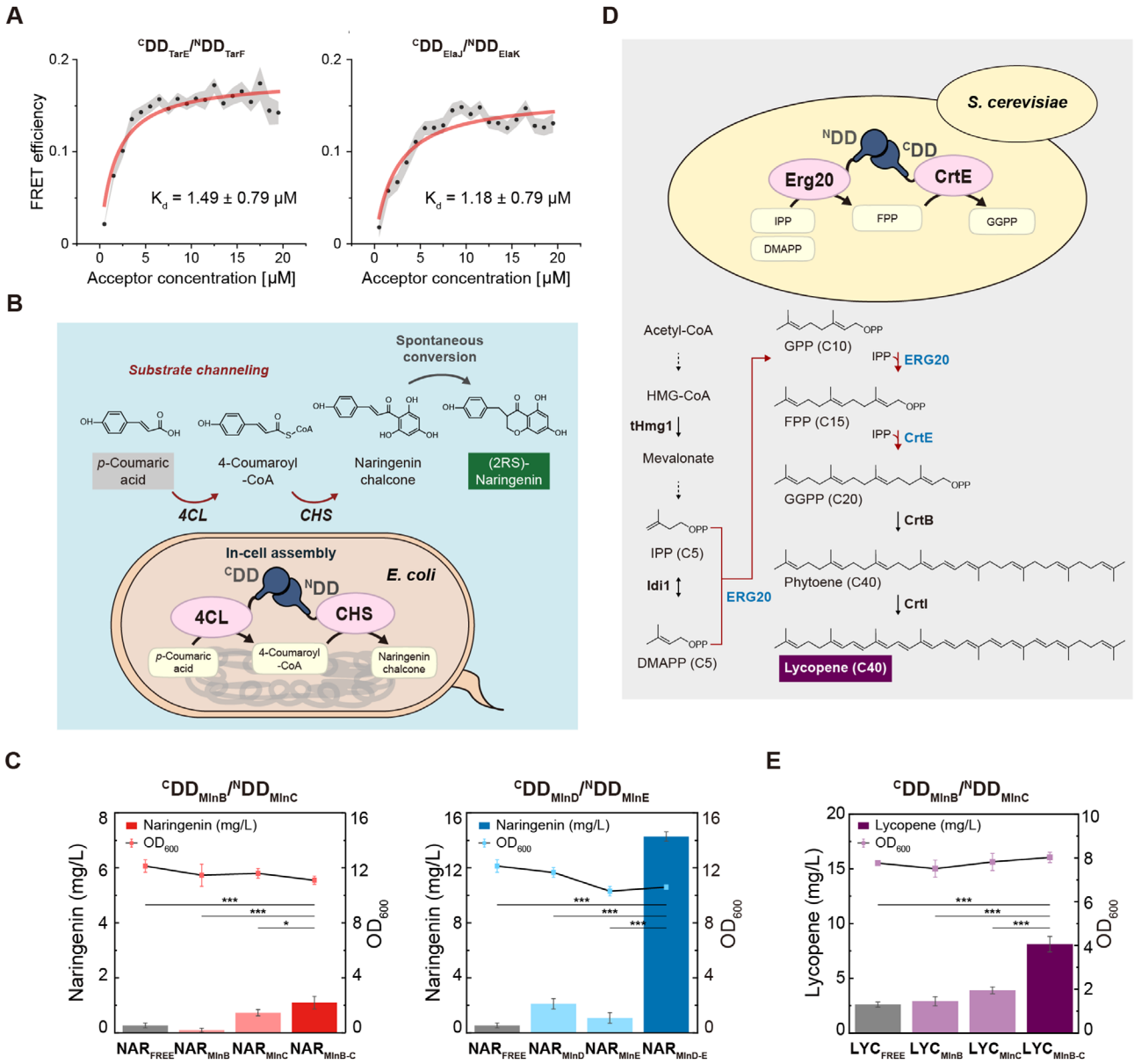

Figure 5. Applications of in-cell K_d measurements using accurate FRET analysis for synthetic biology. A) Representative in-cell K_d measurements of DD pairs, $^{C}DD_{TarE}/^{N}DD_{TarF}$ and $^{C}DD_{ElaJ}/^{N}DD_{ElaK}$. The K_d values were measured to be $1.49 \pm 0.79 \times 10^{-6}$ M for $^{C}DD_{TarE}/^{N}DD_{TarF}$ and $1.18 \pm 0.79 \times 10^{-6}$ M for $^{C}DD_{ElaJ}/^{N}DD_{ElaK}$ using KD-FRET in living *E. coli* cells (mean ± SD). Measurements were performed in triplicate at 37 °C. The gray-shaded regions represent the 95% confidence intervals for the binned mean FRET efficiency. B) Schematic representation of the experimental design for the artificial metabolon system utilizing the enzymes 4-coumaroyl-CoA ligase (4CL) and chalcone synthase (CHS). In this system, *p*-coumaric acid is converted into 4-coumaroyl-CoA by 4CL, followed by the conversion of 4-coumaroyl-CoA into naringenin chalcone by CHS. Finally, naringenin chalcone spontaneously forms (2RS)-naringenin. The metabolon system was constructed by fusing 4CL and CHS with either $^{C}DD_{MlnB}/^{N}DD_{MlnC}$ or $^{C}DD_{MlnD}/^{N}DD_{MlnE}$ pairs, facilitating substrate channeling within *E. coli* cells. C) Naringenin production levels (left *y*-axis, bar graphs) in the artificial metabolon system using the $^{C}DD_{MlnB}/^{N}DD_{MlnC}$ pair (left) and the $^{C}DD_{MlnD}/^{N}DD_{MlnE}$ pair (right). The OD_{600} values of *E. coli* cultures are shown as line graphs (right *y*-axis). The metabolon system utilizing the $^{C}DD_{MlnD}/^{N}DD_{MlnE}$ pair, which exhibited a lower K_d in living cells, resulted in a more significant increase in naringenin production compared to the system using the $^{C}DD_{MlnB}/^{N}DD_{MlnC}$ pair. Measurements were performed in triplicate at 30 °C and error bars reflect standard deviation. Statistical significance was determined using one-way ANOVA followed by Tukey's post-hoc test (***$p < 0.001$, *$p < 0.05$). D) Schematic representation of the experimental design for the artificial metabolon system utilizing the enzymes farnesyl pyrophosphate synthase (FPP synthase, ERG20) and geranylgeranyl pyrophosphate synthase (GGP synthase, CrtE). In this system, ERG20 catalyzes the sequential condensation of isopentenyl pyrophosphate (IPP, C5) with dimethylallyl pyrophosphate (DMAPP, C5), and then with the resultant geranyl pyrophosphate (GPP, C10) to the ultimate product farnesyl pyrophosphate (FPP, C15). And a downstream enzyme CrtE synthesizes geranylgeranyl pyrophosphate (GGPP, C20) from C5-IPP and C15-FPP. ERG20 and CrtE were fused with $^{C}DD_{MlnB}/^{N}DD_{MlnC}$ pair to assemble two enzymes for substrate channeling within *S. cerevisiae* cells. E) Lycopene production levels (left *y*-axis, bar graphs) in the artificial metabolon system using the $^{C}DD_{MlnB}/^{N}DD_{MlnC}$ pair. The metabolon system utilizing the $^{C}DD_{MlnB}/^{N}DD_{MlnC}$ pair resulted in the 3.4-fold increased lycopene production. Measurements were performed in triplicate at 30 °C and error bars reflect standard deviation. Statistical significance was determined using one-way ANOVA followed by Tukey's post-hoc test (***$p < 0.001$).

ing session for each sample. These correction steps were conducted in the same environment as the measurements for the corresponding PPI pairs, ensuring that any potential effect from *E. coli* autofluorescence or environmental variables was effectively accounted for and removed.

In this study, we used only cytosolic proteins, which diffuse freely throughout the *E. coli* cell body. However, if the proteins of interest are membrane proteins that are localized to the cell membrane, the calculation of intracellular concentration becomes more complex, as the system shifts from a 3D to a 2D framework. In such cases, an additional 2D definition of intracellular concentration would be required for K_d calculation.

KD-FRET offers several notable strengths. First, KD-FRET enables PPI quantification using only basic fluorescence microscopy setups, which are commonly available. The simplicity and accessibility of this technique make it broadly applicable to researchers. Moreover, KD-FRET can be readily applied to other bacterial species that meet the following conditions: low autofluorescence in minimal media, controllable expression of fluorescent proteins with genome editing accessibility, free diffusion of proteins without cellular compartmentalization, and the ability to calculate cell volume from 2D images. Based on previous studies, we have identified *Bacillus subtilis*,[50] *Caulobacter crescentus*,[51] *Vibrio cholerae*,[52] and *Streptococcus pneumonia*[53] as suitable candidates for KD-FRET implementation, ensuring reliable intracellular K_d measurements in these species. In principle, the same workflow established in *E. coli*—including transformation, protein expression, and FRET measurements—can be directly applied to these bacteria. Second, KD-FRET allows simultaneous quantification of intracellular protein concentration and FRET efficiency without cell disruption. This feature provides a direct correlation between protein concentration and interaction strength in individual living cells. Third, KD-FRET has a K_d measurement range of ≈0.05–30 × 10^{-6} M (Note S1, Supporting Information), which encompasses the majority of PPIs occurring in *E. coli*.[54] This range makes KD-FRET highly suitable for studying a wide spectrum of biologically significant interactions in live *E. coli* cells.

The KD-FRET method also has certain limitations. As KD-FRET relies on FRET signals for interaction indication, the distance between the donor and acceptor FPs has to be within 7–9 nm in the protein complex. However, this requirement does not constrain the overall size of protein complex. As long as the FPs are properly positioned in a close-proximity within the protein complex, KD-FRET can effectively characterize interactions, even large multi-domain proteins. Another limitation is the need for multiple control samples to perform a series of corrections. Specifically, fluorescent images of two types of cells, one expressing only the donor FP and the other expressing only the acceptor FP, are additionally required.

KD-FRET enables unprecedented quantification of PPIs and accurate determination of FRET efficiency in living bacterial cells by successfully adapting single-molecule FRET analysis to bacterial imaging, overcoming previous limitations of weak FRET signals.[17,20] This method may resolve discrepancies between PPI behaviors in vitro and in living cells, as demonstrated by our finding that certain protein pairs exhibit interactions in cells despite showing no binding in vitro. In addition, the ability to measure K_d in living *E. coli* opens new possibilities for studying how intracellular conditions or external stimuli affect PPIs. For example, KD-FRET can quantify the effects of factors such as antibiotic exposure or metabolic shifts on the strength and stability of protein interactions in living bacterial cells, providing insights into cellular adaptability under diverse environmental conditions. In a similar example, Sukenik et al. quantified weak PPI by cell-volume perturbation in U-2 OS cells.[38] Overall, KD-FRET bridges the gap between in vitro studies and cellular processes, providing crucial insights for drug development, pathogen research, and biotechnology.[55]

4. Experimental Section

Plasmids and Bacterial Strains: Plasmids and bacterial strains used in this work are listed in Tables S1 and S2 (Supporting Information). For in-cell FRET measurement, donor and acceptor vectors were chosen with respect to plasmid incompatibility, usage of different antibiotics for selection, and inducers for individual expression of protein. As a result, pFF838 (p15A origin, chloramphenicol, anhydrotetracycline [aTc]) and pBBR6k (pBBR1 origin, kanamycin, isopropyl β-D-thiogalactopyranoside [IPTG]) were chosen for the donor and acceptor expression vectors, respectively. pFF838 was a gift from Timothy Lu (Addgene plasmid # 61457) and pBBR6k-GFPuv was a gift from Brian Pfleger (Addgene plasmid # 106384). Oligonucleotides for molecular cloning were synthesized by Bionics (Table S1, Supporting Information). The DNA fragments were amplified by Primestar GXL and assembled by the HiFi DNA Assembly strategy. Fluorescent proteins were amplified from pcDNA3.1(+) eGFP, a gift from Jeremy Wilusz (Addgene plasmid # 129020) and pcDNA3-mRFP, a gift from Doug Golenbock (Addgene plasmid # 13032). The *4CL* gene from *Arabidopsis thaliana* and *CHS* gene from *Petunia* × *hybrida* were used to construct the in-cell assembly assays. Short PKS DD DNA fragments with a linker were synthesized by $\text{COSMO}_{\text{GENETECH}}$. The heterologous *crtE* and *crtI* genes from *Xanthophyllomyces dendrorhous* and *crtB* gene from *Pantoea agglomerans* were used for lycopene production in *Saccharomyces cerevisiae* host. For SY002, SY004, and SY007 strains, the lac operon was replaced with Tsr-FP sequence using Lambda-RED recombination using pKD46 as previously described.[56] For SY006 (*uvrA uvrB* double deletion mutant) construction, the Cas9 genome editing technique was used with the procedures that were described elsewhere.[57] The sequence of the plasmid was confirmed by Sanger sequencing (Bionics). *E. coli* strain BW25993 or BL21(DE3) was transformed by the recombinant plasmid for in-cell FRET measurement or protein expression, respectively. *S. cerevisiae* haploid strain CEN.PK2-1C (EUROSCARF 30000A) was used as a parental strain for lycopene production.

Protein Expression and Purification: For protein purification, the expression vector pET21c transformed BL21 (DE3) cells were grown in LB medium containing 50 μg mL^{-1} ampicillin at 37 °C with shaking. Overnight cultures were inoculated into fresh LB media and induced when the culture reached an OD_{600} of 0.6–0.7. The donor protein and eGFPd-mRFP expression plasmids transformants were induced by addition of 1 × 10^{-3} M IPTG at 16 °C and the acceptor protein expression plasmid transformants were induced by addition of 0.5 × 10^{-3} M IPTG at 37 °C. After overnight of induction, the cells were harvested by 6000× *g* 10 min of centrifugation. His-tagged protein expressed cells were resuspended with 20 × 10^{-3} M Tris-HCl (pH 7.4), 400 × 10^{-3} M NaCl, 20 × 10^{-3} M imidazole, 2 × 10^{-3} M 4-benzenesulfonyl fluoride hydrochloride (AEBSF), and 5 × 10^{-3} M 1,4-dithiothreitol (DTT). GST-tagged protein expressed cells were resuspended with PBS, supplemented with 0.5% N-lauroylsarcosine, 2 × 10^{-3} M AEBSF, and 5 × 10^{-3} M DTT. The cells were disrupted by sonication and the crude lysate was centrifuged at 14000× *g* for 30 min at 4 °C. The supernatant was then loaded to Ni-NTA agarose bead (for His-tagged protein) or glutathione-agarose bead (for GST-tagged protein) and incubated for 1.5 h at 4 °C for sufficient bead binding. After several times of washing, His-tagged proteins were eluted by elution buffer (20 × 10^{-3} M Tris-HCl (pH 7.4), 100 × 10^{-3} M NaCl, and 500 × 10^{-3} M imidazole)

and GST-tagged proteins were cleaved from the resin by 30 U of thrombin. The proteins were concentrated by ultrafiltration using Amicon Ultra centrifugal filters.

Cell Growth Condition for K_d Measurement in Living E. Coli Cells: To measure the accurate FRET signal, a single colony was grown overnight in 3 mL of LB medium at 37 °C. Overnight cultures were inoculated 1:100 to M9 medium supplemented with 0.4% glucose and 1× MEM vitamin and 1× MEM amino acids and induced with anhydrotetracycline (pFF838 vector) or/and IPTG (pBBR6k vector) until they reached an OD_{600} of ≈0.3. Following the induction, cells were harvested and transferred to fresh, prewarmed M9 medium supplemented with 0.4% glucose to be OD_{600} of ≈0.1 and grown without inducers for an additional 2 h to allow for the maturation of fluorescent proteins already expressed in cells.[58] For the minimal expression of the SY002, SY004, and SY007 strains, cells were grown in 3 mL of M9 medium supplemented with 0.4% glucose, amino acids, and vitamins at 37 °C. The overnight M9 cultures were inoculated 1:200 into fresh M9 medium same as the overnight culture and grew 5–6 h at 37 °C until they reached an OD_{600} of ≈0.3.

Microscopy: The cells were harvested by centrifugation (6000× *g*, 1 min) and washed with fresh M9 medium supplemented with 0.4% glucose. The cells were then placed on a 3% low melting temperature agarose gel pad (SeaPlaque GTG agarose, Lonza, #50111) and covered with a coverslip. Image acquisition was carried out at a temperature of 37 °C with the aid of a temperature controller (FCS2, Bioptechs). The samples were placed on an inverted microscope (Olympus, IX-71) that was outfitted with a 100× oil-immersed objective lens (Olympus) and further enhanced with a 1.6× amplification. The microscope was used to acquire phase-contrast images and three fluorescence images (donor, acceptor, and FRET channels) at multiple positions using an EMCCD camera (iXon DU888, Andor). For the donor channel, FF02-482/18-25 (excitation), FF01-525/45-25 (emission), and Di03-R488-t1-25 × 36 (dichroic mirror) were used. For the acceptor channel, FF01-572/28-25 (excitation), FF02-641/75-25 (emission), and FF593-Di02-25 × 36 (dichroic mirror) were used. For the FRET channel, FF02-482/18-25 (excitation), FF02-641/75-25 (emission), and FF593-Di02-25 × 36 (dichroic mirror) were used. Semrock provided all the necessary filters. A 488 nm diode laser (LX 150 mW, OBIS) and a 580 nm fiber laser (VFL-P-Series, MPB Communications Inc.) were used to excite the donor and acceptor, respectively. Metamorph software (Molecular Devices) was utilized to automate the measurements.

Image Analysis: The images were analyzed using home-built software (Matlab). The program extracted the total fluorescence intensity, cell size, major and minor axes of individual cells from the phase contrast by identification of the boundaries of individual cells. For in-cell FRET measurements, image background intensity was measured by the mode of intensity per pixel in the image. The wild-type BW25993 strain was used to subtract the autofluorescence of all samples. Donor- and acceptor-only transformed cells were used to calculate the leakage and direct excitation, respectively. The γ factor was calculated by serial imaging SY004 strain before and after mRFP photobleaching. The intensity of the FRET channel of the PPI sample was corrected with the intensity of the background image, autofluorescence, leakage, direct excitation, and γ factor. After the correction, due to the small FRET signal and a series of correction steps, outlier removal was conducted regarding the threshold of the donor channel intensity. To quantify the number of intracellular proteins, minimally expressed SY002 and SY007 strains were imaged under the same imaging condition with the FRET measurements of living *E. coli* cells.

K_d Calculation in Living Cells: For in-cell K_d measurement, acceptor protein concentrations of single cells were binned together as equivalent, and their FRET efficiencies calculated with corrected FRET intensities and donor protein concentrations were averaged. The averaged FRET efficiency was plotted against the binned acceptor protein concentration and the fitted to the quadratic binding equation.

In Vitro K_d Measurement: K_d measurements of the purified proteins were conducted by using Multimode plate reader (Synergy TM H1, BioTek Instruments). The donor channel (Excitation: 475 nm, Emission: 515 nm), the acceptor channel (Excitation: 580 nm, Emission: 607 nm), and the FRET channel (Excitation: 475 nm, Emission: 607 nm) were used. The concentration of the donor protein was fixed to 0 and 1×10^{-6} M and that of the acceptor protein was increased 0 to 20×10^{-6} M. In the case of in vitro K_d calculation, binning of the acceptor protein concentration was unnecessary and the donor protein concentration was fixed to 1×10^{-6} M.

In Vitro FRET Efficiency Measurement of Purified Positive Control: The FRET efficiency can be calculated considering the extinction coefficients of donor and acceptor, as follows:[20,34,59]

$$E = \frac{F_{DA}^{FRET}}{F_{AA}^{FRET}} * \frac{\varepsilon_{A_{ex}}^{A}}{\varepsilon_{D_{ex}}^{D}} \tag{4}$$

where F_{DA}^{FRET} and F_{AA}^{FRET} are the FRET channel intensity and the acceptor channel intensity of sample, respectively. $\varepsilon_{A_{ex}}^{A}$ is the extinction coefficient of the acceptor protein at acceptor excitation wavelength, and $\varepsilon_{D_{ex}}^{D}$ is the extinction coefficient of the donor protein at donor excitation wavelength. Leakage and direct excitation were corrected from the FRET channel intensities using purified eGFPd and mRFP. The intensities of the FRET channel and the acceptor channel of purified samples were measured using a fluorescence spectrophotometer (Cary Eclipse, Agilent). To identify the molar extinction coefficients of eGFPd and mRFP at the wavelengths used in this work, the concentrations of the proteins were determined by a BCA assay, and the absorbance was measured using a UV–vis spectrophotometer (Libra S70, Biochrom).

Isothermal Titration Calorimetry: The ITC sample cell was filled with 400 µL of 80×10^{-6} M eGFPd-$^{C}DD_{MlnB}$, prepared in a buffer containing 20×10^{-3} M Tris-HCl (pH 7.9), 250×10^{-3} M NaCl, 1×10^{-3} M EDTA, 10% (v/v) glycerol, and 1×10^{-3} M TCEP. Using a micro-syringe, 2 µL of 1.6×10^{-3} M $^{N}DD_{MlnC}$-mRFP was injected into the sample cell at 400 s intervals with gentle stirring. A total 20 injections were titrated for each measurement. All experiments were performed at 37 °C using the Affinity ITC instruments (TA Instruments, New Castle, DE). The experimental data were fitted assuming a single binding site model.

Metabolic Assays in E. Coli and S. Cerevisiae: Plasmids and strains for in-cell assay of 4CL-CHS assembly mediated by DD pairs are listed in Tables S2 and S3 (Supporting Information). For comparison, constructs of 4CL-CHS combinations were also prepared for cases without DD and with only acceptor DD or donor DD. The relevant plasmids were transformed into *E. coli* BW25993 for naringenin production. The recombinant *E. coli* strains were grown in LB medium supplemented with 50 µg mL^{-1} kanamycin at 37 °C until an OD600 of 0.8. The cells were re-cultured in 50 mL of YM9 medium (6.8 g of Na_2HPO_4, 3 g of KH_2PO_4, 0.5 g of NaCl, 1 g of NH_4Cl, 10 g of yeast extract, 30 mL of glycerol, 42 g of MOPS (pH 7.0) per liter) supplemented with 50 µg mL^{-1} kanamycin at 37 °C. After an OD600 of 0.8 had been reached, the expression was induced with 0.1×10^{-3} M IPTG, and 1×10^{-3} M *p*-coumaric acid was added as the initial substrate for naringin biosynthesis, followed by incubation at 30 °C for 40 h. To analyze naringenin production, the culture broth was extracted with twice the volume of ethyl acetate and evaporated to dryness, and the extracts were dissolved in methanol. Samples were analyzed by ultra-performance liquid chromatography (UPLC)–quadrupole time-of-flight high-resolution mass spectrometry (qTOF-HR-MS), as described in a previous work.[60] Independent experiments were performed three or more times.

Plasmids and strains for assembly of lycopene pathway enzymes are listed in Tables S2 and S3 (Supporting Information). For lycopene production, *S. cerevisiae* strains were cultivated in synthetic complete (SC) medium containing 20 g L^{-1} glucose, 6.7 g L^{-1} yeast nitrogen base without amino acids, and a suitable concentration of amino acid dropout mixture for plasmid selection. Seed cultures were initiated by inoculating yeast cells harboring plasmids into 5 mL of selective SC medium in a 50-mL flask, followed by incubation at 30 °C for 24 h with shaking at 170 rpm. Subsequently, 10 mL of selective SC medium in a 100-mL flask was inoculated with the seed culture at an initial OD_{600} of 0.2 and incubated under the same conditions for 120 h. Lycopene extraction was performed using a customized hot-HCl method. Cultured yeast cells were resuspended in 1 N HCl and lysed by alternating boiling and cooling cycles. Specifically, the cells were subjected to 7 min of boiling, followed by 3 min on ice, an-

other 7 min of boiling, and a final 5 min on ice. After cooling, the lysed cells were washed with triple-distilled water (TDW) and collected by centrifugation for 3 min. Lycopene was extracted by adding an appropriate volume of HPLC-grade acetone to the cell pellet, followed by vortexing for 5 min. Cell debris was removed by centrifugation for 5 min, and the resulting supernatant was used for lycopene quantification. Lycopene quantification was performed using an UltiMate 3000 HPLC system (Thermo Fisher Scientific) equipped with an Agilent Eclipse XDB-C18 column (250 mm × 4.6 mm, 5 µm, Agilent, Santa Clara, CA). Filtered samples were analyzed with a mobile phase composed of dichloromethane:acetonitrile:methanol in a ratio of 16:42:42, at a flow rate of 1.2 mL min^{-1}. Lycopene detection was achieved using a UV–visible detector set to a wavelength of 471 nm. The column temperature was maintained at 30 °C throughout the analysis.

Statistical Analysis: All experiments were performed in triplicate, and the results are presented as mean ± standard deviation (SD). The K_d values were determined by fitting the FRET efficiency versus acceptor concentration data to a quadratic binding equation using nonlinear regression analysis. For plotting the KD-FRET data, 95% confidence intervals were calculated and displayed as shaded regions to represent the variability within each bin. For naringenin production experiments, statistical significance was determined using one-way ANOVA followed by Tukey's post-hoc test. *P*-values less than 0.05 were considered statistically significant.

All statistical analyses and graph plotting were performed using Origin 2023b (OriginLab, Northampton, MA) or Microsoft Excel 2016 software.

Supporting Information

Supporting Information is available from the Wiley Online Library or from the author.

Acknowledgements

This research was supported by the Samsung Research Funding and Incubation Center of Samsung Electronics under project number SRFC-MA1802-10.

Conflict of Interest

The authors declare no conflict of interest.

Author Contributions

S.Y. and E.K. contributed equally to this work. S.Y., E.K., Y.J.Y., and N.K.L. conceived and designed the study. S.Y., S.Y., and E.K. performed FRET measurements and analyzed the data. E.K., G.K., and J.-S.H. conducted artificial metabolon experiments and data analysis. J.S.J. and H.H.L. carried out the ITC experiments. D.-W.B., S.-Y.S., B.-G.J., and S.-S.C. contributed to data analysis. S.Y., E.K., J.-S.H., Y.J.Y., and N.K.L. wrote the manuscript, which was reviewed and approved by all authors for the final version. Y.J.Y. and N.K.L. supervised the project.

Data Availability Statement

The data that support the findings of this study are available from the corresponding author upon reasonable request.

Keywords

biosensor, FRET, living cells, protein–protein interactions, synthetic biology

Received: November 12, 2024
Revised: February 26, 2025
Published online: March 24, 2025

[1] a) K. M. Poluri, K. Gulati, D. K. Tripathi, N. Nagar, *Protein-Protein Interactions*, Springer Nature, Berlin **2023**; b) S. V. Rajagopala, P. Sikorski, A. Kumar, R. Mosca, J. Vlasblom, R. Arnold, J. Franca-Koh, S. B. Pakala, S. Phanse, A. Ceol, R. Hauser, G. Siszler, S. Wuchty, A. Emili, M. Babu, P. Aloy, R. Pieper, P. Uetz, *Nat. Biotechnol.* **2014**, *32*, 285; c) F. M. Paulussen, G. K. Schouten, C. Moertl, J. Verheul, I. Hoekstra, G. M. Koningstein, G. H. Hutchins, A. Alkir, R. A. Luirink, D. P. Geerke, P. van Ulsen, T. den Blaauwen, J. Luirink, T. N. Grossmann, *J. Am. Chem. Soc.* **2022**, *144*, 15303; d) T. A. Cameron, W. Margolin, *Nat. Rev. Microbiol.* **2024**, *22*, 33; e) S. Rudolf, K. Kaempf, O. Vu, J. Meiler, A. G. Beck-Sickinger, I. Coin, *Angew. Chem., Int. Ed.* **2022**, *61*, e202108738.

[2] a) G. Papadakos, A. Sharma, L. E. Lancaster, R. Bowen, R. Kaminska, A. P. Leech, D. Walker, C. Redfield, C. Kleanthous, *J. Am. Chem. Soc.* **2015**, *137*, 5252; b) S. Bhattacharyya, S. Bershtein, J. Yan, T. Argun, A. I. Gilson, S. A. Trauger, E. I. Shakhnovich, *Elife* **2016**, *5*, e20309; c) H. Lu, Q. Zhou, J. He, Z. Jiang, C. Peng, R. Tong, J. Shi, *Signal Transduction Targeted Ther.* **2020**, *5*, 213.

[3] M. R. Arkin, A. Whitty, *Curr. Opin. Chem. Biol.* **2009**, *13*, 284.

[4] a) N. K. Aghera, J. Prabha, H. Tandon, G. Chattopadhyay, S. Vishwanath, N. Srinivasan, R. Varadarajan, *Structure* **2020**, *28*, 562; b) P. Hariharan, D. Balasubramaniam, A. Peterkofsky, H. R. Kaback, L. Guan, *Proc. Natl. Acad. Sci. USA* **2015**, *112*, 2407.

[5] S. L. Speer, W. Zheng, X. Jiang, I. T. Chu, A. J. Guseman, M. Liu, G. J. Pielak, C. Li, *Proc. Natl. Acad. Sci. USA* **2021**, *118*, e2019918118.

[6] a) I. Piazza, K. Kochanowski, V. Cappelletti, T. Fuhrer, E. Noor, U. Sauer, P. Picotti, *Cell* **2018**, *172*, 358; b) M. Tabaka, T. Kalwarczyk, J. Szymanski, S. Hou, R. Holyst, *Front. Phys.* **2014**, *2*, 54; c) D. de Sancho, A. Sirur, R. B. Best, *Nat. Commun.* **2014**, *5*, 4307; d) A. P. Minton, *J. Cell. Sci.* **2006**, *119*, 2863; e) S. Chung, E. Lerner, Y. Jin, S. Kim, Y. Alhadid, L. W. Grimaud, I. X. Zhang, C. M. Knobler, W. M. Gelbart, S. Weiss, *Nucleic Acids Res.* **2019**, *47*, 1440; f) D. G. Rattray, L. J. Foster, *Curr. Opin. Chem. Biol.* **2019**, *48*, 81.

[7] T. C. Jarvis, D. M. Ring, S. S. Daube, P. H. Vonhippel, *J. Biol. Chem.* **1990**, *265*, 15160.

[8] a) S. Xing, N. Wallmeroth, K. W. Berendzen, C. Grefen, *Plant Physiol.* **2016**, *171*, 727; b) A. G. Ngounou Wetie, I. Sokolowska, A. G. Woods, U. Roy, K. Deinhardt, C. C. Darie, *Cell. Mol. Life Sci.* **2014**, *71*, 205.

[9] a) A. M. Edwards, B. Kus, R. Jansen, D. Greenbaum, J. Greenblatt, M. Gerstein, *Trends Genet.* **2002**, *18*, 529; b) H. N. Lin, V. W. Cornish, *Angew. Chem.,Int. Ed.* **2001**, *40*, 871.

[10] J. Mehla, J. H. Caufield, N. Sakhawalkar, P. Uetz, in *Methods in Enzymology*, Vol. *586* (Ed: A. K. Shukla), Academic Press, San Diego, CA **2017**, pp. 333–358.

[11] Y. Hu, K. Cheng, L. He, X. Zhang, B. Jiang, L. Jiang, C. Li, G. Wang, Y. Yang, M. Liu, *Anal. Chem.* **2021**, *93*, 1866.

[12] a) E. J. Osterlund, N. Hirmiz, J. M. Pemberton, A. Nougarede, Q. Liu, B. Leber, Q. Fang, D. W. Andrews, *Sci. Adv.* **2022**, *8*, eabm7375; b) X. Shi, R. Lingerak, C. J. Herting, Y. Ge, S. Kim, P. Toth, W. Wang, B. P. Brown, J. Meiler, K. Sossey-Alaoui, M. Buck, J. Himanen, D. Hambardzumyan, D. B. Nikolov, A. W. Smith, B. Wang, *Science* **2023**, *382*, 1042; c) B. Liu, O. J. Stone, M. Pablo, J. C. Herron, A. T. Nogueira, O. Dagliyan, J. B. Grimm, L. D. Lavis, T. C. Elston, K. M. Hahn, *Cell* **2021**, *184*, 5670.

[13] D. C. Youvan, W. J. Coleman, C. M. Silva, E. J. Bylina, M. R. Dilworth, M. M. Yang, *Biotechnology* **1997**, *3*, 1.

[14] G. W. Gordon, G. Berry, X. H. Liang, B. Levine, B. Herman, *Biophys. J.* **1998**, *74*, 2702.

[15] Z. Xia, Y. Liu, *Biophys. J.* **2001**, *81*, 2395.

[16] A. Coullomb, C. M. Bidan, C. Qian, F. Wehnekamp, C. Oddou, C. Albiges-Rizo, D. C. Lamb, A. Dupont, *Sci. Rep.* **2020**, *10*, 6504.

[17] X. You, A. W. Nguyen, A. Jabaiah, M. A. Sheff, K. S. Thorn, P. S. Daugherty, *Proc. Natl. Acad. Sci. USA* **2006**, *103*, 18458.

[18] V. Sourjik, H. C. Berg, *Proc. Natl. Acad. Sci. USA* **2002**, *99*, 12669.
[19] T. Lin, B. L. Scott, A. D. Hoppe, S. Chakravarty, *Prot. Sci.* **2018**, *27*, 1850.
[20] N. K. Lee, A. N. Kapanidis, Y. Wang, X. Michalet, J. Mukhopadhyay, R. H. Ebright, S. Weiss, *Biophys. J.* **2005**, *88*, 2939.
[21] G. Agam, C. Gebhardt, M. Popara, R. Machtel, J. Folz, B. Ambrose, N. Chamachi, S. Y. Chung, T. D. Craggs, M. de Boer, D. Grohmann, T. Ha, A. Hartmann, J. Hendrix, V. Hirschfeld, C. G. Hubner, T. Hugel, D. Kammerer, H. S. Kang, et al., *Nat. Methods* **2023**, *20*, 523.
[22] R. P. Novick, *Microbiol. Rev.* **1987**, *51*, 381.
[23] G. N. van der Krogt, J. Ogink, B. Ponsioen, K. Jalink, *PLoS One* **2008**, *3*, e1916.
[24] a) C. Wu, M. Mori, M. Abele, A. Banaei-Esfahani, Z. Zhang, H. Okano, R. Aebersold, C. Ludwig, T. Hwa, *Nat. Microbiol.* **2023**, *8*, 347; b) A. Schmidt, K. Kochanowski, S. Vedelaar, E. Ahrne, B. Volkmer, L. Callipo, K. Knoops, M. Bauer, R. Aebersold, M. Heinemann, *Nat. Biotechnol.* **2016**, *34*, 104.
[25] a) J. B. Son, S. Kim, S. Yang, Y. Ahn, N. K. Lee, *J. Phys. Chem. B* **2024**, *128*, 6730; b) S. Yang, S. Kim, D. K. Kim, H. J. An, J. B. Son, A. H. Gynna, N. K. Lee, *Nat. Commun.* **2019**, *10*, 5131.
[26] C. Berney, G. Danuser, *Biophys. J.* **2003**, *84*, 3992.
[27] a) T. Ha, J. Fei, S. Schmid, N. K. Lee, R. L. Gonzalez, S. Paul, S. Yeou, *Nat. Rev. Methods Primers* **2024**, *4*, 21; b) B. Hellenkamp, S. Schmid, O. Doroshenko, O. Opanasyuk, R. Kuhnemuth, S. Rezaei Adariani, B. Ambrose, M. Aznauryan, A. Barth, V. Birkedal, M. E. Bowen, H. Chen, T. Cordes, T. Eilert, C. Fijen, C. Gebhardt, M. Gotz, G. Gouridis, E. Gratton, et al., *Nat. Methods* **2018**, *15*, 669.
[28] a) H. Chen, H. L. Puhl III, S. V. Koushik, S. S. Vogel, S. R. Ikeda, *Biophys. J.* **2006**, *91*, L39; b) T. Zal, N. R. Gascoigne, *Biophys. J.* **2004**, *86*, 3923.
[29] a) T. Ha, A. Y. Ting, J. Liang, W. B. Caldwell, A. A. Deniz, D. S. Chemla, P. G. Schultz, S. Weiss, *Proc. Natl. Acad. Sci. USA* **1999**, *96*, 893; b) J. J. McCann, U. B. Choi, L. Zheng, K. Weninger, M. E. Bowen, *Biophys. J.* **2010**, *99*, 961.
[30] B. Epe, K. G. Steinhauser, P. Woolley, *Proc. Natl. Acad. Sci. USA* **1983**, *80*, 2579.
[31] S. Yang, S. Kim, Y. R. Lim, C. Kim, H. J. An, J. H. Kim, J. Sung, N. K. Lee, *Nat. Commun.* **2014**, *5*, 4761.
[32] I. Jarmoskaite, I. AlSadhan, P. P. Vaidyanathan, D. Herschlag, *Elife* **2020**, *9*, e57264.
[33] A. Plochowietz, R. Crawford, A. N. Kapanidis, *Phys. Chem. Chem. Phys.* **2014**, *16*, 12688.
[34] R. M. Clegg, *Methods Enzymol.* **1992**, *211*, 353.
[35] S. Y. Son, D. W. Bae, E. Kim, B. G. Jeong, M. Y. Kim, S. Y. Youn, S. Yi, G. Kim, J. S. Hahn, N. K. Lee, Y. J. Yoon, S. S. Cha, *Structure* **2024**, *32*, 1477.
[36] J. L. Meinke, A. J. Simon, D. T. Wagner, B. R. Morrow, S. You, A. D. Ellington, A. T. Keatinge-Clay, *ACS Synth. Biol.* **2019**, *8*, 2017.
[37] a) S. B. Zimmerman, S. O. Trach, *J. Mol. Biol.* **1991**, *222*, 599; b) A. P. Minton, *J. Biol. Chem.* **2001**, *276*, 10577; c) Y. Phillip, V. Kiss, G. Schreiber, *Proc. Natl. Acad. Sci. USA* **2012**, *109*, 1461.
[38] S. Sukenik, P. Ren, M. Gruebele, *Proc. Natl. Acad. Sci. USA* **2017**, *114*, 6776.
[39] D. Pakotiprapha, M. Samuels, K. Shen, J. H. Hu, D. Jeruzalmi, *Nat. Struct. Mol. Biol.* **2012**, *19*, 291.
[40] a) E. S. Day, S. M. Cote, A. Whitty, *Biochemistry* **2012**, *51*, 9124; b) S. Brudar, B. Hribar-Lee, *J. Phys. Chem. B* **2021**, *125*, 2504; c) S. O. Ugwu, S. P. Apte, *Pharm. Tech.* **2004**, *28*, 86; d) M. R. Arkin, M. A. Glicksman, H. Fu, J. J. Havel, Y. Du, in *Assay Guidance Manual*, Eli Lilly & Company and the National Center for Advancing Translational Sciences, Bethesda, MD **2004**. e) R. Moussa, A. Baierl, V. Steffen, T. Kubitzki, W. Wiechert, M. Pohl, *J. Biotechnol.* **2014**, *191*, 250.
[41] a) D. Roberts, R. Keeling, M. Tracka, C. F. van der Walle, S. Uddin, J. Warwicker, R. Curtis, *Mol. Pharm.* **2015**, *12*, 179; b) P. Singh, A. Roche, C. F. van der Walle, S. Uddin, J. Du, J. Warwicker, A. Pluen, R. Curtis, *Mol. Pharm.* **2019**, *16*, 4775; c) A. Salis, L. Cappai, C. Carucci, D. F. Parsons, M. Monduzzi, *J. Phys. Chem. Lett.* **2020**, *11*, 6805.
[42] a) J. Zeng, D. T. Wagner, Z. Zhang, L. Moretto, J. D. Addison, A. T. Keatinge-Clay, *ACS Chem. Biol.* **2016**, *11*, 2466; b) S. I. Elshahawi, A. E. Trindade-Silva, A. Hanora, A. W. Han, M. S. Flores, V. Vizzoni, C. G. Schrago, C. A. Soares, G. P. Concepcion, D. L. Distel, E. W. Schmidt, M. G. Haygood, *Proc. Natl. Acad. Sci. USA* **2013**, *110*, E295.
[43] a) J. Behrendorff, G. Borras-Gas, M. Pribil, *Trends Biotechnol.* **2020**, *38*, 432; b) V. Pareek, Z. Sha, J. He, N. S. Wingreen, S. J. Benkovic, *Mol. Cell.* **2021**, *81*, 3775.
[44] a) Y. Zhang, S. Z. Li, J. Li, X. Pan, R. E. Cahoon, J. G. Jaworski, X. Wang, J. M. Jez, F. Chen, O. Yu, *J. Am. Chem. Soc.* **2006**, *128*, 13030; b) C. J. Delebecque, A. B. Lindner, P. A. Silver, F. A. Aldaye, *Science* **2011**, *333*, 470; c) J. E. Dueber, G. C. Wu, G. R. Malmirchegini, T. S. Moon, C. J. Petzold, A. V. Ullal, K. L. J. Prather, J. D. Keasling, *Nat. Biotechnol.* **2009**, *27*, 753; d) R. J. Conrado, G. C. Wu, J. T. Boock, H. Xu, S. Y. Chen, T. Lebar, J. Turnsek, N. Tomsic, M. Avbelj, R. Gaber, T. Koprivnjak, J. Mori, V. Glavnik, I. Vovk, M. Bencina, V. Hodnik, G. Anderluh, J. E. Dueber, R. Jerala, M. P. DeLisa, *Nucleic Acids Res.* **2012**, *40*, 1879.
[45] a) Y. Zang, J. Zha, X. Wu, Z. Zheng, J. Ouyang, M. A. G. Koffas, *J. Agric. Food Chem.* **2019**, *67*, 13430; b) D. Liu, M. S. Sica, J. Mao, L. F. Chao, V. Siewers, *ACS Synth. Biol.* **2022**, *11*, 3228.
[46] Z. Serber, R. Ledwidge, S. M. Miller, V. Dotsch, *J. Am. Chem. Soc.* **2001**, *123*, 8895.
[47] a) B. Wallace, P. J. Atzberger, *PLoS One* **2017**, *12*, e0177122; b) L. Barbieri, E. Luchinat, L. Banci, *Sci. Rep.* **2015**, *5*, 14456.
[48] a) G. Karimova, J. Pidoux, A. Ullmann, D. Ladant, *Proc. Natl. Acad. Sci. USA* **1998**, *95*, 5752; b) J. K. Joung, E. I. Ramm, C. O. Pabo, *Proc. Natl. Acad. Sci. USA* **2000**, *97*, 7382.
[49] a) D. S. Burz, K. Dutta, D. Cowburn, A. Shekhtman, *Nat. Methods* **2006**, *3*, 91; b) J. Xie, R. Thapa, S. Reverdatto, D. S. Burz, A. Shekhtman, *J. Med. Chem.* **2009**, *52*, 3516.
[50] a) R. McQuillen, A. J. Perez, X. Yang, C. H. Bohrer, E. L. Smith, S. Chareyre, H.-C. T. Tsui, K. E. Bruce, Y. M. Hla, J. W. McCausland, M. E. Winkler, E. D. Goley, K. S. Ramamurthi, J. Xiao, *Nat. Commun.* **2024**, *15*, 10746; b) M. Tišma, F. P. Bock, J. Kerssemakers, H. Antar, A. Japaridze, S. Gruber, C. Dekker, *Nat. Commun.* **2024**, *15*, 2737.
[51] a) A. Persat, H. A. Stone, Z. Gitai, *Nat. Commun.* **2014**, *5*, 3824; b) J. Deich, E. M. Judd, H. H. McAdams, W. E. Moerner, *Proc. Natl. Acad. Sci. USA* **2004**, *101*, 15921.
[52] S. Vaidya, D. Saha, D. K. H. Rode, G. Torrens, M. F. Hansen, P. K. Singh, E. Jelli, K. Nosho, H. Jeckel, S. Göttig, F. Cava, K. Drescher, *Nat. Microbiol.* **2025**, *10*, 144.
[53] a) A. J. Perez, Y. Cesbron, S. L. Shaw, J. Bazan Villicana, H. T. Tsui, M. J. Boersma, Z. A. Ye, Y. Tovpeko, C. Dekker, S. Holden, M. E. Winkler, *Proc. Natl. Acad. Sci. USA* **2019**, *116*, 3211; b) M. Kjos, R. Aprianto, V. E. Fernandes, P. W. Andrew, J. A. G. v. Strijp, R. Nijland, J.-W. Veening, *J. Bacteriol.* **2015**, *197*, 807.
[54] J. R. Perkins, I. Diboun, B. H. Dessailly, J. G. Lees, C. Orengo, *Structure* **2010**, *18*, 1233.
[55] a) D. Schultz, M. Stevanovic, L. S. Tsimring, *Biophys. J.* **2022**, *121*, 4137; b) M. Liu, A. Mirza, P. C. McAndrew, A. Thapaliya, O. A. Pierrat, M. Stubbs, T. Hahner, N. E. A. Chessum, P. Innocenti, J. Caldwell, M. D. Cheeseman, B. R. Bellenie, R. L. M. van Montfort, G. K. Newton, R. Burke, I. Collins, S. Hoelder, *J. Med. Chem.* **2023**, *66*, 10617.
[56] K. A. Datsenko, B. L. Wanner, *Proc. Natl. Acad. Sci. USA* **2000**, *97*, 6640.

[57] J. Y. Seok, Y. H. Han, J. S. Yang, J. Yang, H. G. Lim, S. G. Kim, S. W. Seo, G. Y. Jung, *Cell Rep.* **2021**, *36*, 109589.
[58] a) D. C. Prasher, V. K. Eckenrode, W. W. Ward, F. G. Prendergast, M. J. Cormier, *Gene* **1992**, *111*, 229; b) E. Balleza, J. M. Kim, P. Cluzel, *Nat. Methods* **2018**, *15*, 47.
[59] V. Mekler, E. Kortkhonjia, J. Mukhopadhyay, J. Knight, A. Revyakin, A. N. Kapanidis, W. Niu, Y. W. Ebright, R. Levy, R. H. Ebright, *Cell* **2002**, *108*, 599.
[60] M. S. Xiao, J. E. Wilusz, *Nucleic Acids Res.* **2019**, *47*, 8755.